REDVET - Revista electrónica de Veterinaria - ISSN 1695-7504
Vol 25, No. 1 (2024)
http://www.veterinaria.org
Article Received: Revised: Accepted:

Antimicrobial Activity, Physicochemical, And Spectral Analysis Of Rare Earth Metal Complexes Derived From N"-[(Z)-(3-Fluorophenyl)Methylidene]-N"-[(1E,2E)-[Hydroxylamine-1,2-Diphenylidene]Thiocarbohydrazide

Sharad Sankhe[1*] and Shashank Parab[1]

[1*]Department of Chemistry, Patkar-Varde College, Goregaon West, Mumbai-62, India.

Abstract
The biologically active ligand N"-[(Z)-(3-fluorophenyl)methylidene]-N"-[(1E,2E)-[hydroxylamine-1,2-diphenylidene] thiocarbohydrazide (HBMT*m*FB) was synthesized via a condensation reaction involving α-benzilmonoximethio carbohydrazide and *m*-fluorobenzaldehyde in the presence of a catalytic quantity of HCl. This HBMT*m*FB ligand serves as the precursor for the preparation of lanthanide metal complexes. A series of trinuclear lanthanide complexes [Ln(BMT*m*FB)$_3$] were synthesized, encompassing ten distinct compounds featuring different lanthanide ions such as La(III), Yb(III), Dy(III), Lu(III), Ce(III), Ho(III), Pr(III), Sm(III), Nd(III), and Gd(III). The chemical functionalities of these complexes were extensively characterized using UV-visible and infrared spectroscopy, proton magnetic resonance (PMR) spectroscopy, elemental analysis (C, H, N, S), magnetic susceptibility measurements, and molar conductivity studies. The coordination behavior of HBMT*m*FB as a tridentate, monobasic ligand was elucidated, with its two oxygen, two sulfur, and nitrogen atoms forming a coordination sphere capable of interacting with metal ions, as confirmed by infrared spectroscopy. Furthermore, the antibacterial activity of the synthesized metal complexes was assessed successfully.

Keywords: α-Benzilmonoximethiocarbohydrazide, infrared spectroscopy, Molar conductivity, lanthanide metal complexes.

1. Introduction:

The biomedical implications of lanthanides remain relatively unexplored, despite their promising pharmacological attributes [1-3]. Although extensively studied and characterized chemically, lanthanides offer intriguing avenues for future investigation in the coming years [4]. Metal ions play pivotal roles in the mechanisms of action of pharmaceuticals [5], engaging in diverse interactions with antibiotics, proteins, lipid components, nucleic acids, and other biomolecules [6-9]. Metal complexes can modulate the toxicological and pharmacological profiles of various drugs [10]. Among these, Gd(III) ions have been extensively researched and found utility in numerous therapies, including as constituents of MRI contrast agents. The diverse chemical and magnetic properties of lanthanide(III) ion-based lanthanide complexes hold particular significance in cancer diagnostics and therapy. The study of lanthanides and their compounds has garnered significant attention in recent years due to their profound applications in medicinal inorganic chemistry and materials science. Lanthanide complexes serve as contrast agents in medical imaging, particularly magnetic resonance imaging (MRI), and are increasingly vital in various diagnostic modalities and as radiotherapeutic agents [11-12]. Lanthanide ions possess exceptional redox stability, rendering them highly suitable for cellular use in the presence of biological reducing agents such as ascorbate and thiols. Moreover, they exhibit favorable luminescent properties attributed to 4f↔5d, charge transfer, and *f*↔*f* transitions [13]. Researchers intrigued by recent developments in medicinal chemistry are exploring the potential medical applications of lanthanides. These advancements motivate further investigation into the coordination behavior of HBMT*m*FB with lanthanide metal ions. This paper presents insights into the synthesis, characterization, and antibacterial properties of the HBMT*m*FB ligand and its lanthanide metal complexes.

2. Materials and Methods:

The experimental procedures employed analytical-grade chemicals and glassware. Lanthanide (III) metal nitrates, including those of lanthanum, lutetium, cerium, holmium, ytterbium, dysprosium, samarium, and gadolinium, as well as the *m*-fluorobenzaldehyde ligand, were of high purity. High-quality solvents suitable for spectroscopic analysis were utilized for recording spectra. Bacterial strains such as *Escherichia coli* (*E. coli*), *Pseudomonas aeruginosa* (*P. aeruginosa*), *Staphylococcus aureus* (*S. aureus*), and *Bacillus subtilis* (*B. subtilis*) were employed for antibacterial screening, while *Candida albicans* (*C. albicans*) and *Saccharomyces cerevisiae* (*S. cerevisiae*) were used for antifungal screening. Melting point determination and thin-layer chromatography (TLC) using a hexane and ethyl acetate solvent mixture (8:2 ml ratio) were conducted for the ligand and complexes. The ligand exhibited a melting point of 145.5 ˚C, while the complexes displayed melting temperatures exceeding 360 ˚C. Conductivity measurements were performed using a Zeal Tech conductometer with a cell constant of 1±10% cm^{-1}. Molar conductance was determined using 10^{-3} M solutions of metal chelates in nitrobenzene solvent. Carbon and hydrogen microanalysis was conducted using a THERMO FINNIGAN CHNS analyzer. The concentrations of lanthanum (III), lutetium (III), cerium (III), samarium (III), neodymium (III), holmium (III), ytterbium (III), dysprosium (III), praseodymium (III), and gadolinium (III) were

calculated using the EDTA back titration method. Infrared spectra of inner transition complexes and the ligand were obtained using a Bruker FT-IR spectrophotometer operating in the range of 4000-400 cm^{-1}. Magnetic susceptibility of solid metal-ligand chelate complexes was determined using Gouy's method at 293 K, with $Hg[Co(CNS)_4]$ serving as a calibrant. Electronic spectra of complexes were acquired using a JASCO V650 UV-vis spectrophotometer. The antibacterial activity of the synthesized complexes was evaluated by determining minimal inhibitory concentrations through disc diffusion methods.

2.1. Synthesis of HBMT*m*FB ligand:

The synthesis of the HBMT*m*FB ligand involved the condensation reaction between α-benzilmonoximethio carbohydrazide (10 mmol) and *m*-fluorobenzaldehyde (10 mmol) in ethanol. The resulting reaction mixture was refluxed for 5 hours, cooled, and allowed to stand overnight at room temperature. The yellow solid product was isolated by filtration and washed with hot distilled water.

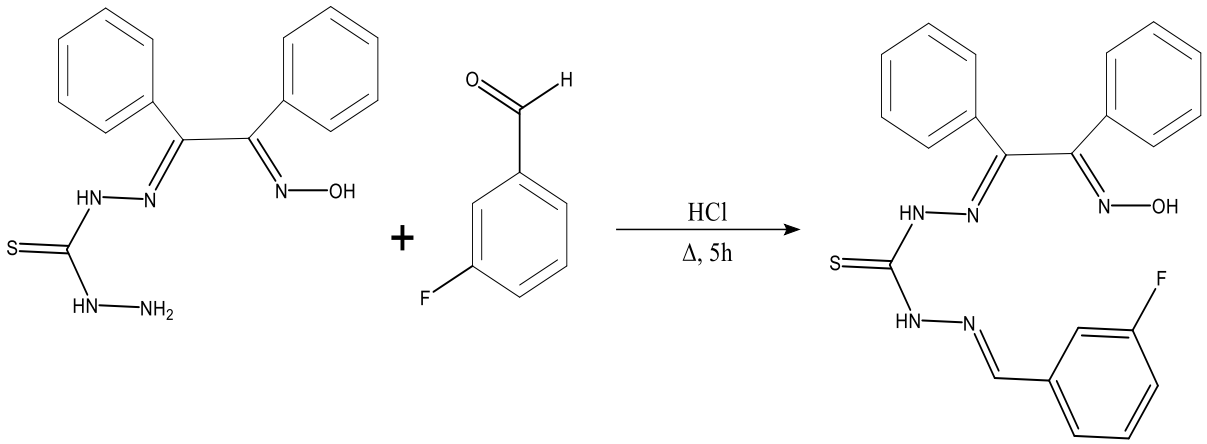

Scheme 1: Preparation of HBMT*m*FB ligand

2.2. Synthesis and rare metal complexes:

The metal complexes were synthesized by mixing a 15 mmol solution of metal nitrate with a 5 mmol solution of HBMT*m*FB ligand dissolved in ethanol. The molar ratio between the ligand and metal was maintained at 3:1. The resulting mixture was refluxed for 3 hours at a temperature of 60°C. After the reflux period, the mixture was cooled and stirred for approximately 1 hour, during which no precipitation occurred. To facilitate precipitation of the complex, the pH of the reaction mixture was adjusted to 7 by adding a 0.1 M NaOH solution, creating a nearly neutral environment. The resulting metal chelate precipitates were filtered and washed with alcohol to remove any residual unreacted metal and ligand. Finally, the product was dried in an oven at 50˚C. This synthesis procedure was employed for all the complexes.

2.3. Antibacterial Screening:

Through the disc diffusion method, we evaluated the antibacterial properties of the compounds by assessing their impact on the growth response of various microbes *in vitro*. To activate the bacterial strains, a 30 ml nutrient broth was inoculated with a loop full of the provided test strain and then allowed to incubate in a 30 °C incubator for 24 hours. Subsequently, 20 ml of nutrient agar medium was poured into Petri dishes with a diameter of 120 mm. Once the agar reached a temperature of 37 °C, 0.1 ml of the activated strain was added to it, and the media were allowed to solidify. Sterile filter paper discs (6 mm in diameter) were then placed in the Petri dishes for both the samples and the standard drug kanamycin (30 µg/disc). As a control, pure solvent was applied to the discs in the Petri dishes, and the test samples were applied using a micropipette under aseptic conditions. This process was repeated for each bacterial strain and solvent. The Petri dishes were then incubated at 37 °C for 24 hours. The effectiveness of the synthetic complexes against the tested bacterial strains was assessed by measuring the inhibition zone that formed between the two chemicals. The extent of growth inhibition was determined by measuring the diameter of zones exhibiting complete inhibition (in mm) in comparison to the positive control.

2.4. Minimum Inhibitory Concentration (MIC):

The minimum inhibitory concentration (MIC) of the test compounds against the same bacteria used for antibacterial screening was determined using the serial tube dilution technique. Nutrient agar medium was employed for this purpose. The test compounds were serially diluted twofold from the stock solution to generate solutions with decreasing concentrations. Each tube was inoculated with 10 µl of a bacterial suspension containing 10^7 cells/ml. Following incubation at 37 °C for one day, the MIC value of the sample in µg/ml was determined by identifying the test tube in which no microbial growth was observed.

REDVET - Revista electrónica de Veterinaria - ISSN 1695-7504
Vol 25, No. 1 (2024)
http://www.veterinaria.org
Article Received: Revised: Accepted:

2.5. Brine shrimp lethality bioassay:

Following the established protocol [19], the cytotoxic effects of the investigated substances were assessed. *Brine shrimp* (*Artemia salina*) eggs were incubated in seawater for 48 hours at room temperature with continuous aeration. The seawater was prepared by dissolving 38 g of NaCl in 1 L of distilled water. Subsequently, the compounds were diluted to 5 ml with seawater, and stock solutions of the complexes (10 mg/ml in DMSO) were added to each vial, resulting in final concentrations of 0, 20, 40, 60, 80, and 100 µg/ml. Ten live shrimp were then introduced into each vial and left undisturbed for one day. The number of surviving nauplii in each vial was counted and recorded.

3. Results and Discussion:

The ligand HBMTmFB was utilized for the synthesis of complexes with lanthanide metal ions, including La(III), Lu(III), Ce(III), Sm(III), Nd(III), Ho(III), Yb(III), Dy(III), Pr(III), and Gd(III). These complexes underwent characterization using various analytical techniques. Notably, they displayed significant solubility in dimethyl sulfoxide (DMSO) and complete solubility in dimethylformamide (DMF) and nitrobenzene, while being insoluble in methanol, ethanol, acetonitrile, and ethyl acetate. Moreover, the complexes of La(III), Lu(III), Ce(III), Sm(III), Nd(III), Ho(III), Yb(III), Dy(III), Pr(III), and Gd(III) demonstrated non-hygroscopic properties. Magnetic susceptibility measurements were conducted using Gouy's method, revealing that the magnetic moment of lanthanide metal ions remains consistent irrespective of the surrounding ligands, making it indistinguishable between different coordination geometries [20]. The molar conductance of the metal complexes was also evaluated, yielding values ranging from 0.259 to 1.428 $\Omega^{-1}cm^2mol^{-1}$. The presence of the mol^{-1} indication indicates that all synthesized complexes are non-electrolytic.

Table 1: Analytical and physical data of the ligand and its lanthanide (III) metal complexes

Compound	Color	Yield %	M.P. / Dec. pointºC	Elemental Analysis							Magnetic Moments (B.M.)	Electrical Conductance 10^{-3} M(in NB) mhos
				% M Found (Calcd)	% C Found (Calcd)	% H Found (Calcd)	% N Found (Calcd)	% O Found (Calcd)	% S Found (Calcd)	% F Found (Calcd)		
HBMT*m*FB	Yellow	77.69	191	-	62.96 (62.90)	4.22 (4.27)	16.60 (16.65)	3.77 (3.78)	7.55 (7.56)	4.51 (4.53)	-	-
[La(BMT*m*FB)$_2$]	Yellow	81.54	202	10.29 (10.32)	56.71 (56.78)	3.64 (3.65)	15.00 (15.03)	3.40 (3.41)	6.80 (6.80)	4.07 (4.08)	Dia	0.99
[Dy(BMT*m*FB)$_2$]	White	77.47	210	10.69 (10.77)	55.88 (55.91)	3.55 (3.60)	14.81 (14.83)	3.37 (3.39)	6.77 (6.78)	4.00 (4.02)	10.39	1.06
[Gd(BMT*m*FB)$_2$]	White	76.89	207	10.59 (10.65)	55.93 (56.12)	3.50 (3.61)	14.87 (14.88)	3.33 (3.40)	6.79 (6.80)	3.99 (4.00)	7.92	1.25
[Nd(BMT*m*FB)$_2$]	White	77.23	205	10.27 (10.32)	56.62 (56.64)	3.55 (3.65)	14.99 (15.02)	3.40 (3.43)	6.85 (6.87)	4.06 (4.08)	3.09	0.54
[Sm(BMT*m*FB)$_2$]	Yellow	76.49	206	10.66 (10.79)	56.36 (56.40)	3.58 (3.63)	14.93 (14.95)	3.41 (3.42)	6.82 (6.84)	4.05 (4.06)	3.63	1.55
[Lu(BMT*m*FB)$_2$]	Green	80.11	209	13.91 (14.03)	52.16 (52.23)	3.32 (3.36)	13.82 (13.85)	3.12 (3.17)	6.32 (6.33)	3.73 (3.76)	Dia	1.76
[Pr(BMT*m*FB)$_2$]	White	81.24	208	10.16 (10.20)	56.74 (56.78)	3.64 (3.66)	15.01 (15.05)	3.42 (3.44)	6.86 (6.88)	4.04 (4.09)	3.57	1.50
[Ce(BMT*m*FB)$_2$]	Yellow	77.68	211	10.00 (10.05)	52.76 (52.81)	3.63 (3.66)	15.02 (15.06)	3.44 (3.44)	6.81 (6.83)	4.03 (4.09)	1.86	1.68
[Ho(BMT*m*FB)$_2$]	L. Brown	79.33	209	14.07 (14.13)	52.27 (52.31)	3.57 (3.59)	14.66 (14.79)	3.33 (3.38)	6.76 (6.78)	4.00 (4.01)	10.30	1.39

3.1. IR spectra:

The binding mechanism of the ligand HBMT*m*FB to Ln(III) ions in these complexes was investigated by comparing the Fourier-transform infrared (FT-IR) spectrum of HBMT*m*FB with that of its Ln(III) complexes. In the FT-IR spectrum of the HBMT*m*FB ligand, two prominent absorption bands were observed at 1615 cm^{-1} and 1565 cm^{-1}, corresponding to the (C=NN) and (C=NO) stretching vibrations of the azomethine and oximino groups, respectively. Upon complexation with Ln(III) ions, the characteristic bands of the ligand HBMT*m*FB in the infrared spectra of all Ln(III) complexes exhibited shifts in various directions, as summarized in **Table 2**. The similarities in the infrared spectrum shifts among the various complexes suggest that the Ln(III) complexes possess comparable structures. The disappearance of the band observed at 3287 cm^{-1} in the IR spectra of the ligand indicated the deprotonation of the oximino group upon metal-ligand complex formation. Additionally, new bands observed in the complex IR spectra at 563-619 cm^{-1}, 530-577 cm^{-1}, and 506-533 cm^{-1} were attributed to the stretching vibrations of M-O, M□N, and M□S, respectively. The absence of these bands in the ligand spectrum confirms the involvement of metal ions in lanthanide HBMT*m*FB chelates, connecting with the azomethine nitrogen, thiocarbonyl sulfur, and oximino oxygen ions.

Table 2: IR spectral bands of the ligand (HBMT*m*FB) and its metal complexes (cm^{-1}):

Assignments	HBMH*m*CB	La(III)	Ce(III)	Pr(III)	Nd(III)	Sm(III)	Gd(III)	Ho(III)	Yb(III)	Dy(III)	Lu(III)

νOH Oximino	3287	-	-	-	-	-	-	-	-	-	-
N-H	3165	3160	3155	3261	3261	3262	3260	3261	3261	3260	3313
νCH	2959	2978	2978	2979	2979	2978	2977	2979	2978	2977	2835
νC=NN	1615	1514	1486	1514	1514	1514	1513	1514	1514	1515	1493
νC=NO	1565	1486	1459	1486	1488	1486	1485	1487	1488	1487	1467
νC=S	1243	1232	1232	1231	1232	1232	1231	1232	1232	1232	1235
νM-O	-	567	618	619	618	618	615	580	618	620	563
νM-N	-	535	572	577	577	567	563	537	577	575	530
νM→N	-	514	534	534	536	533	516	506	517	525	509

3.2. Electronic Spectral study:

Table 3 presents the UV-visible absorption spectrum data for the HBMT*m*FB ligand and its complexes, detailing the maximum absorption wavelength (λ_{max}) and corresponding band assignments. The samples, prepared at a concentration of 10^{-6} M using DMF as the solvent, were subjected to spectrum recording at room temperature. The HBMT*m*FB ligand exhibits absorption peaks at 275 and 390 nm, attributed to n→π* transitions arising from conjugation between the lone pair of electrons of sulfur atoms and the π electrons of the thiocarbonyl group (C=S). The La(III) complex displays absorption bands in the visible range at 400-450 and 475-490 nm, ascribed to charge transfer (CT) transitions (L→M and M→L) between La(III) and the ligand. Additionally, weaker bands observed between 572 and 688 nm indicate d-d transitions of La(III) ($^2B_{1g}\rightarrow{}^2E_g$). The Sm(III) complex bands may be attributed to *4f-4f* transitions between ground and excited states ($^6H_{5/2}$ to $^4F_{3/2}$, $^4F_{9/2}$, $^6F_{11/2}$, and $^4G_{5/2}$). Gadolinium (III) complex exhibits *f-f* transition bands at 690 nm and 448.50 nm, corresponding to *4f-4f* transitions from the ground state $^8S_{7/2}$ to excited states of $^6D_{5/2}$. The Ce(III) complex displays distinct absorption bands at 455 and 428 nm, indicating charge transfer phenomena. The observed magnetic moment of the Ce(III) complex (1.83 B.M.) deviates from standard experimental values due to antiferromagnetic interaction. The Dy(III) complex excitation spectrum exhibits narrow bands (330-425 nm) attributed to $^4f_9$ intra-configurational transitions. The Ho(III) complex absorption spectrum reveals multiplet-to-multiplet conversions from the ground state to stimulated states within the range of 370 to 680 nm, with significant sensitivity observed at 443 nm. Praseodymium (III) complex absorption bands result from transitions between ground and excited *J* levels of the *4f* configuration. The systematic red-shift in electronic spectra of the complexes indicates the presence of covalent bonding, implying complex stoichiometry as [Ln(BMT*m*FB)$_3$], supported by absorption spectra, magnetic characteristics, and chemical analysis.

3.3. NMR spectra:

The singlet observed at δ 12.147 ppm in the ligand's 1H NMR spectra is likely attributed to the oximino proton. Its absence in the diamagnetic lanthanum(III) complexes' spectra suggests that oximino oxygen participates in chelation post deprotonation. Proton signals from aliphatic amine moiety and phenyl ring (manifesting as two sets of singlets at δ 12.477 and 10.145 ppm) in lanthanum(III) complexes' spectra do not exhibit any relocation. This observation suggests that the electric environment surrounding these sites, situated a few bonds away from the metal ion, remains unchanged by weak metal-ligand interactions.

3.4. Powder X-ray diffraction:

Due to the substantial molecular mass of the metal ions, obtaining single crystals of these complexes was unsuccessful, prompting the collection of powder X-ray diffraction patterns to characterize their crystalline nature. Attempts to index the diffraction patterns using autoindexing computer programs have yet to yield satisfactory unit-cell parameters, likely due to the bulky chelate molecules resulting in larger unit cells and complex symmetry arrangements. Analysis of the data indicates that the metal ions coordinate through the oximino oxygen, thiocarbonyl sulfur, and azomethine nitrogen, achieving a coordination number of nine. Based on the physicochemical and spectroscopic data, the lanthanide (III) complexes of N"-[(Z)-(3-Fluorophenyl)methylidene]-N"-[(1E,2E)-[hydroxylamine-1,2-diphenylidene] thiocarbohydrazide are proposed to have a monocapped trigonal prism geometry.

3.5. Biological Activities:

Table 5 presents the antibacterial activity results of the compounds, assessed by measuring the zone of inhibition. The test compounds exhibited significant sensitivity when tested against various pathogenic bacteria, showing comparable potency to the standard antibiotic kanamycin (30 µg/disc).

For the Nd(III) complex, its effectiveness against all tested bacterial species was similar to that of kanamycin. Moreover, when tested at higher doses (100 µg/disc and 200 µg/disc), slightly improved outcomes were observed. Meanwhile, the Sm(III), Pr(III), and Gd(III) complexes demonstrated moderate activity even at higher doses. Notably, the solvent DMSO did not inhibit any bacterial strain. The minimum inhibitory concentration (MIC) values of the test compounds, listed in **Table 5**, were calculated in µg/ml.

The compounds' cytotoxic effects were assessed through brine shrimp lethality assays to determine the median lethal concentration (LC50) by analyzing the correlation between sample concentration and percentage of death. The LC50 values for Sm(III), Lu(III), Pr(III), and Ho(III) were found to be 50 µg/ml, 45 µg/ml, 60 µg/ml, and 40 µg/ml, respectively.

REDVET - Revista electrónica de Veterinaria - ISSN 1695-7504
Vol 25, No. 1 (2024)
http://www.veterinaria.org
Article Received: Revised: Accepted:

4. Conclusions:

These nine Schiff base complexes of inner transition metals, synthesized from N"-[(Z)-(3-Fluorophenyl)methylidene]-N"-[(1E,2E)-[hydroxylamine-1,2-diphenylidene] thiocarbohydrazide, were prepared using a straightforward, rapid, and effective method. The structures proposed in Figure 1 are based on the observed nine-coordinated geometries from the preceding study. Thermal and IR data confirm the coordination of molecules in these metal complexes. They exhibit non-electrolytic behavior, possess distinctive colors, and decompose at elevated temperatures. The antimicrobial activity of all synthesized compounds was investigated, revealing potent antibacterial properties. Additionally, cytotoxic effects were observed for all chemicals. Thus, further investigations employing advanced technologies could lead to the development of these molecules as novel antibacterial agents.

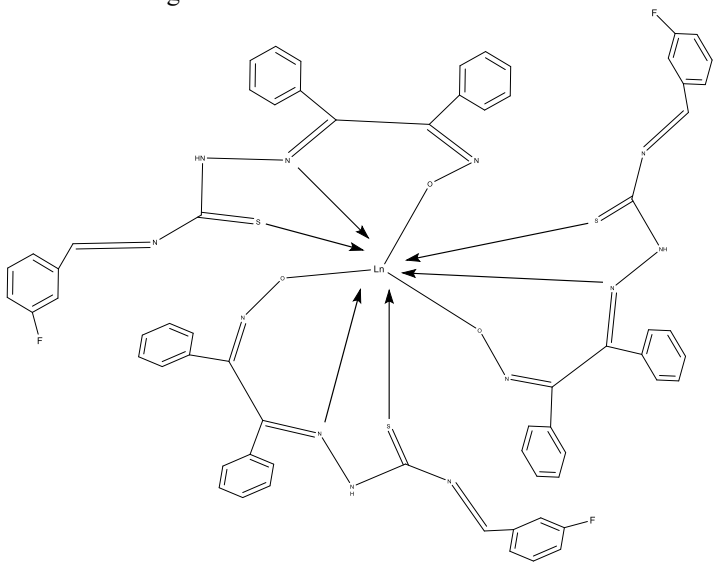

References:

1. Fouad, R. (2020). Synthesis and characterization of lanthanide complexes as potential therapeutic agents. *Journal of Coordination Chemistry*, *73*(14), 2015-2028.
2. Ajlouni, A. M., Abu-Salem, Q., Taha, Z. A., Hijazi, A. K., & Al Momani, W. (2016). Synthesis, characterization, biological activities and luminescent properties of lanthanide complexes with [2-thiophenecarboxylic acid, 2-(2-pyridinylmethylene) hydrazide] Schiff bases ligand. *Journal of rare earths*, *34*(10), 986-993.
3. Georgieva, I., Mihaylov, T., & Trendafilova, N. (2014). Lanthanide and transition metal complexes of bioactive coumarins: Molecular modeling and spectroscopic studies. *Journal of Inorganic Biochemistry*, *135*, 100-112.
4. Mishra, N., Kumar, K., Pandey, H., Anand, S. R., Yadav, R., Srivastava, S. P., & Pandey, R. (2020). Synthesis, characterization, optical and anti-bacterial properties of benzothiazole Schiff bases and their lanthanide (III) complexes. *Journal of Saudi Chemical Society*, *24*(12), 925-933.
5. Chundawat, N. S., Jadoun, S., Zarrintaj, P., & Chauhan, N. P. S. (2021). Lanthanide complexes as anticancer agents: A review. *Polyhedron*, *207*, 115387.
6. Staszak, K., Wieszczycka, K., Marturano, V., & Tylkowski, B. (2019). Lanthanides complexes–Chiral sensing of biomolecules. *Coordination Chemistry Reviews*, *397*, 76-90.
7. Mattocks, J. A., & Cotruvo, J. A. (2020). Biological, biomolecular, and bio-inspired strategies for detection, extraction, and separations of lanthanides and actinides. *Chemical Society Reviews*, *49*(22), 8315-8334.
8. Chundawat, N. S., Jadoun, S., Zarrintaj, P., & Chauhan, N. P. S. (2021). Lanthanide complexes as anticancer agents: A review. *Polyhedron*, *207*, 115387.
9. Shahraki, S., Shiri, F., Heidari Majd, M., & Dahmardeh, S. (2019). Anti-cancer study and whey protein complexation of new lanthanum (III) complex with the aim of achieving bioactive anticancer metal-based drugs. *Journal of Biomolecular Structure and Dynamics*, *37*(8), 2072-2085.
10. Chundawat, N. S., Jadoun, S., Zarrintaj, P., & Chauhan, N. P. S. (2021). Lanthanide complexes as anticancer agents: A review. *Polyhedron*, *207*, 115387.
11. Patyal, M., Kaur, K., Bala, N., Gupta, N., & Malik, A. K. (2023). Innovative Lanthanide Complexes: Shaping the future of cancer/tumor Chemotherapy. *Journal of Trace Elements in Medicine and Biology*, 127277.
12. Gill, M. R., & Vallis, K. A. (2019). Transition metal compounds as cancer radiosensitizers. *Chemical Society Reviews*, *48*(2), 540-557.
13. Wang, L., Zhao, Z., Wei, C., Wei, H., Liu, Z., Bian, Z., & Huang, C. (2019). Review on the electroluminescence study of lanthanide complexes. *Advanced Optical Materials*, *7*(11), 1801256.

14. Matharu, K., Mittal, S. K., & Kumar, S. A. (2011). A novel method for the determination of individual lanthanides using an inexpensive conductometric technique. *Analytical Methods*, *3*(6), 1290-1295.
15. Saunderson, A. (1968). A permanent magnet Gouy balance. *Physics Education*, *3*(5), 272.
16. Saha, N., & Bhattacharyya, D. (1976). Chelates of Cu (II), Ni (II) & Co (II) with 3, 5-Dimethylpyrazole-I-acetic Acid.
17. A. W. Bauer, W. M. M. Kirby, J. C. Sherries, M. Truck, Am. J. Clin. Path. 44 (1966) 493-497.
18. E. Jawetz, J. L. Melnick, E. A. Adelberg., Lange, Medical Pub. 14th ed., California, 1980, p. 123-124.
19. Atta-ur-Rahman, M. I. Choudhary, W. J. Thomsen., Harwood Academic Press, Amsterdam, 1999, p. 12-22.
20. Shebl, M., Khalil, S. M., & Al-Gohani, F. S. (2010). Preparation, spectral characterization and antimicrobial activity of binary and ternary Fe (III), Co (II), Ni (II), Cu (II), Zn (II), Ce (III) and UO2 (VI) complexes of a thiocarbohydrazone ligand. *Journal of Molecular Structure*, *980*(1-3), 78-87.
21. Ferenc, W., Cristóvão, B., & Sarzyński, J. (2013). Magnetic, thermal and spectroscopic properties of lanthanide (III) 2-(4-chlorophenoxy) acetates, Ln (C8H6ClO3) 3• nH2O. *Journal of the Serbian Chemical Society*, *78*(9), 1335-1349.
22. Wei, D. Y., Zheng, Y. Q., & Lin, J. L. (2002). Two Hydroxo Bridged Dinuclear Lanthanide Phen Complexes:[Ln2 (phen) 4 (H2O) 4 (OH) 2](phen) 2 (NO3) 4 with Ln= Tm, Yb. *Zeitschrift für Naturforschung B*, *57*(6), 625-630.
23. Al-Zaidi, B. H., Hasson, M. M., & Ismail, A. H. (2019). New complexes of chelating Schiff base: Synthesis, spectral investigation, antimicrobial, and thermal behavior studies. *Journal of Applied Pharmaceutical Science*, *9*(4), 045-057.
24. Guo, H., Wang, Y., Li, G., Liu, J., Feng, P., & Liu, D. (2017). Cyan emissive super-persistent luminescence and thermoluminescence in BaZrSi 3 O 9: Eu 2+, Pr 3+ phosphors. *Journal of Materials Chemistry C*, *5*(11), 2844-2851.
25. P. Singla, V. Luxami and K. Paul, Eur. J. Med. Chem., 2016, 117, 59
26. Jorgensen, C.K., Prog. Inorg. Chem., 1962, vol. 4, p. 73.
27. Silverstein, R.M., Bassler, G.C., and Morrill, T.C., Spectrometric Identification of Organic Compounds, New York: Wiley, 1981.